J|A|C|S
ARTICLES
Published on Web 08/31/2002

Magnetic Ordering in Doped $Cd_{1-x}Co_xSe$ Diluted Magnetic Quantum Dots

Khalid M. Hanif, Robert W. Meulenberg, and Geoffrey F. Strouse*

Contribution from the Department of Chemistry, University of California, Santa Barbara, California 93106

Received March 22, 2002

Abstract: In this study, we report structural, vibrational, and magnetic data providing evidence of random ion displacement in the core of CdSe quantum dots on the Cd^{2+} sites by Co^{2+} ions (between $x = 0$ and 0.30). Structural evidence for core doping is obtained by analyzing the powder X-ray diffraction (pXRD), data which exhibits a linear lattice compression with increasing Co^{2+} concentration, in accord with Vegard's law. Correlated with the pXRD shift, a hardening of the CdSe longitudinal optical phonon mode and a new local vibrational mode are observed which track Co^{2+} doping concentration. Consistent with the observed core doping, superconducting quantum interference device (SQUID) measurements indicate a surprising increase for the onset of spin glass behavior by an order of magnitude over bulk Co:CdSe. Correlation of SQUID results, pXRD, and Raman measurements suggests that the observed enhancement of magnetic superexchange between Co^{2+} dopant ions in this confined system arises from changes in the nature of coupling in size-restricted materials.

Introduction

Bulk diluted magnetic semiconductors (DMSs) have recently received attention due to their potential usage in magnetic applications including spintronics, magnetic switching, and magnetic recording.[1,2] In DMS materials, the interaction of lattice, spin, and electronic degrees of freedom between the lattice core and the dopant ions can induce paramagnetic (PM), spin-glass (SG), antiferromagnetic (AFM), or ferromagnetic (FM) behavior, depending on the magnitude of d−d (J) and sp−d (α,β) exchange integrals between the paramagnetic dopant and host lattice.[1,3] The magnitude of the orbital mixing can be accounted for in terms of the orbital mixing arising from hybridization between delocalized band electrons in the p valence orbitals and the localized d-orbitals for the paramagnetic ion in a tetrahedral crystal field.[4,5] In II−VI materials, magnetic coupling for Fe, Mn, and Co DMS materials has been observed. In II−VI nanomaterials, Mn^{2+}-doped CdS nanocrystals have shown evidence for size-dependent magnetism.[6] Co^{2+}-doped II−VI systems exhibit stronger coupling due to the increased Co d-orbital mixing with the valence band and conduction band of the II−VI host. For Co^{2+}-doped materials, the p−d hybridization gives rise to long-range AFM coupling via a superexchange mechanism.

In the dilute limit ($x < 0.01$), the dopant spins can be treated as isolated domains, resulting in PM behavior for the DMS system. As the dopant concentration increases, the onset of dopant−dopant spin interactions, arising primarily from nearest-neighbor coupling (J_{NN}) via a superexchange mechanism, causes deviations from the classical PM behavior and the observation of a magnetic SG AFM regime. The onset temperature of SG behavior in the magnetization data has been interpreted as a signature of the magnitude of nearest-neighbor (NN) interactions of the dopant ions within the lattice.[1] At higher concentrations, cobalt-doped DMS systems have been observed to exhibit a type III AFM lattice, arising from strong spin coupling due to strong exchange between Co^{2+} and Se atoms in the hexagonal lattice.[3]

Several researchers have investigated the effects of quantum confinement on the exchange interactions in DMS systems.[7−11] At the nanoscale level, changes in electron−phonon (el−ph) and electron−electron (el−el) interactions may perturb magnetic ordering and lead to exchange properties that show strong size dependencies. Efros and co-workers have shown that incorporation of Mn^{2+} into CdS quantum dots (QDs) leads to a giant internal magnetic field, with a commensurate Zeeman splitting of the electron and hole levels as high as 100 meV, *in the*

* Address correspondence to this author. E-mail: strouse@chem.ucsb.edu.

(1) Furdyna, J. K. *J. Appl. Phys.* **1988**, *64*, R29−R64.
(2) Wolf, S. A.; Awschalom, D. D.; Buhrman, R. A.; Daughton, J. M.; von Molnar, S.; Roukes, M. L.; Chtchelkanova, A. Y.; Treger, D. M. *Science* **2001**, *294*, 1488−1495.
(3) Twardowski, A.; Swagten, H. J. M.; Dejonge, W. J. M. In *Cobalt-based II−VI semimagnetic semiconductors*; Jain, M., Ed.; World Scientific: Singapore, 1993; pp 227−254.
(4) Swagten, H. J. M.; Twardowski, A.; de Jonge, W. J. M.; Demianiuk, M. *Phys. Rev. B* **1989**, *39*, 2568−2577.
(5) Shand, P. M.; Lewicki, A.; Crooker, B. C.; Giriat, W.; Furdyna, J. K. *J. Appl. Phys.* **1990**, *67*, 5246−5248.
(6) Feltin, N.; Levy, L.; Ingert, D.; Pileni, M. P. *Adv. Mater.* **1999**, *11*, 398−402.
(7) Hoffman, D. M.; Meyer, B. K.; Ekimov, A. I.; Merkulov, I. A.; Efros, A. L.; Rosen, M.; Couino, G.; Gacoin, T.; Boilot, J. P. *Solid State Commun.* **2000**, *114*, 547−550.
(8) Mikulec, F. V.; Kuno, M.; Bennati, M.; Hall, D. A.; Griffin, R. G.; Bawendi, M. G. *J. Am. Chem. Soc.* **2000**, *122*, 2532−2540.
(9) Norris, D. J.; Yao, N.; Charnock, F. T.; Kennedy, T. A. *Nano Lett.* **2001**, *1*, 3−7.
(10) Ladizhansky, V.; Vega, S. *J. Phys. Chem. B* **2000**, *104*, 5237−5241.
(11) Radovanovic, P. V.; Gamelin, D. R. *J. Am. Chem. Soc.* **2001**, *123*, 12207−12214.

absence of an external applied magnetic field.[7] In a related experiment on Mn^{2+}-doped CdSe QDs, Bawendi and co-workers optically detected the incorporation of a Mn^{2+} ion into a CdSe host by observing the excitonic fine splitting using fluorescence line narrowing (FLN) and electron spin resonance (ESR) techniques.[8] These results were similar to previous magnetic field-dependent FLN studies on undoped CdSe QDs,[12] leading the authors to speculate that the Mn^{2+} dopant ion acted as a localized magnetic field inside the CdSe QD lattice. The observed hyperfine splitting from the ESR experiments led to speculation that the Mn^{2+} ion sits on a Cd site internally doped near the surface of the QD. Similarly, Norris and co-workers have observed Mn^{2+} doping in ZnSe QDs with hyperfine splitting values leading to speculation about core ion doping.[9] Recent ^{113}Cd NMR studies on Co^{2+}-doped CdS QDs suggest that strong sp−d mixing is achieved, assignable to Co exchange interactions in the core.[10]

The lack of synthetic control over the paramagnetic ion concentration on core Cd^{2+} sites limits the ability to probe the influence of quantum confinement on spin exchange and sp−d mixing in these materials. For QD materials, proof of core doping is crucial to the analysis of these novel dilute magnetic systems. The magnitude of the doping level and the net magnetic behavior of the materials will be dependent on the site of substitution, the degree of lattice mismatch, and charge compensation issues. In a recent study on Co^{2+} CdS QDs, the majority of dopant sites were found to reside on the surface of the QD rather than internal core sites, based on analysis of the crystal field splitting behavior observed in absorption spectra for a series of $Cd_{1-x}Co_xS$.[11] Controlled doping at internal core vs external surface sites in bulk materials is a long-standing issue for these materials. The random displacement of the core atoms by the guest ion can be tracked by analyzing the average change in the lattice parameters by pXRD measurements. According to Vegard's law, the observed average lattice compression or lattice expansion, which correlates with the guest ion radius, should exhibit a linear relationship with the concentration of the guest ion.

In this study, we investigate the structural and magnetic properties of diluted magnetic semiconductor quantum dots (DMQDs), more specifically $Cd_{1-x}Co_xSe$ quantum dots, where $0.001 < x < 0.30$. Based upon powder X-ray diffraction data (pXRD) and resonance Raman spectroscopy, we show evidence for the incorporation of Co^{2+} ions into the wurtzite CdSe lattice. More importantly, the spin-glass temperature for these materials is an order of magnitude higher than that for bulk Co:CdSe DMS. Experimentally, this can be analyzed as an enhancement of the superexchange interactions within the lattice and enhanced contributions from next-nearest-neighbor (NNN) and next-next-nearest-neighbor (NNNN) interactions for confined materials. This suggests that stronger sp−d mixing occurs for these dimensionally restricted materials, perhaps arising from enhanced β contributions due to particle reconstruction. We envision that these DMQDs may represent the next logical step in quantum computing applications via spintronics.

Experimental Section

Synthesis. (a) Materials. The clusters $[Cd_{10}Se_4(SC_6H_5)_{16}](NMe_4)_4$ and $[Co_4(SC_6H_5)_{16}]Li_2$ were prepared by literature methods.[13] Cobalt(II) nitrate hexahydrate (Allied), elemental selenium (Aldrich), thiophenol (Aldrich), hexadecylamine (Aldrich), pyridine (Fisher), $(NMe_4)Cl$ (Aldrich), CH_3OH (Fisher), and CH_3CN (Fisher) were used as supplied.

(b) Synthesis of Co^{2+}-Doped CdSe Quantum Dots. Synthesis of the $Cd_{1-x}Co_xSe$ quantum dots was performed under airless conditions using lyothermal methods based on a single source precursor methodology.[14] Briefly, a cadmium selenide thiolate cluster, $[Cd_{10}Se_4(SC_6H_5)_{16}](NMe_4)_4$ (1.8 g, 0.7 mmol), and a cobalt thiolate cluster, $[Co_4(SC_6H_5)_{10}](NMe_4)_2$ (from 400 mg to 1.25 g, 0.3−0.8 mmol), were combined and heated between 170 and 210 °C in ~40 mL of hexadecylamine (HDA) under N_2. Control of the stoichiometric ratio between the Cd and Co clusters allows control of the doping concentrations in the final product. Quantum dot growth was monitored by UV−vis absorption, and the product was isolated at absorption values corresponding to 50 Å CdSe (first exciton absorbance at 590 nm; 2.1 eV). The QDs were isolated by cooling the reaction mixture to 60 °C, followed by precipitation from HDA via the addition of anhydrous CH_3OH to produce selectively precipitated samples of HDA surface passivated Co:CdSe. To ensure the removal of excess surface-bound Co^{2+} species, the CdSe samples were stripped with pyridine (3×) and recapped with HDA. The Co^{2+} concentration was verified by inductively coupled plasma atomic emission (ICP-AE). Particle size (rms ~5%) for the Co:CdSe samples was determined by UV−vis absorption and transmission electron microscopy (TEM) measurements.

Characterization. (a) Powder X-ray Diffraction (pXRD). Powder X-ray diffraction measurements were measured on a Scintag X2 diffractometer using Cu Kα radiation ($\lambda = 1.5418$ Å). Si powder was used as an internal standard. The Si standard peaks arising at 1.6, 1.9, and 3.1 Å are identified by an asterisk (∗), while the diffraction peaks resulting from the hexadecylamine (HDA) are identified with a dot (●) in Figure 3a. Not all traces show HDA impurities due to batch-to-batch differences in nanocrystal cleaning. The lattice parameters are extracted by fitting to a wurtzite lattice model and have been verified by a Reitveld refinement analysis.[15]

(b) Transmission Electron Microscopy (TEM). TEM analysis was obtained on a JEOL 2010 microscope operated at 200 kV in bright-field mode using Ni-backed holey carbon TEM grids (SPI) with the Formvar removed. Size and size distribution measurements were obtained on a statistical subset of QDs by manual calculation of the QD images obtained by digitizing the micrograph negatives. Comparison of lattice spacing from TEM to pXRD for individual dots is obtained by measuring the fringes in the TEM spacing.

(c) Photoluminescence and Resonance Raman Spectroscopy. The photoluminescence (PL) and resonance Raman spectra (resonant with a high-energy $1P_h1P_e$ transition) were collected in backscattering configuration using the 2.54 eV (488.0 nm) line of a 10W Spectra-Physics 2200 (Raman; 80mW) or an American Laser Corp. (PL; 10 mW) Ar ion laser as a pump source. The Raman spectra were collected on a 0.5 M ARC single spectrograph (1800 lines mm^{-1}, blaze = 500 nm) system coupled to a Princeton Instruments 512 × 512 liquid nitrogen–cooled charge-coupled device (CCD) array. The PL experiments were measured on a 0.5 M CVI single spectrograph (150 lines mm^{-1}, blaze = 500 nm) coupled to an air-cooled 375 × 242 CCD array (Santa Barbara Instrument Group). The peaks in the Raman spectra at ~310 cm^{-1} are laser plasma lines and are marked with an asterisk (∗). In both experiments, a holographic notch filter (Kaiser optical) was used to reject the incident laser line.

(d) UV−Vis Spectroscopy. UV−vis absorption measurements were measured with an Ocean Optics S2000 CCD fiber-optic spectrophotometer (resolution 4 meV). All measurements were taken at room temperature.

(12) Nirmal, M.; Norris, D. J.; Kuno, M.; Bawendi, M. G.; Efros, A. L.; Rosen, M. *Phys. Rev. Lett.* **1995**, *75*, 3728−3731.
(13) Dance, I. G.; Choy, A.; Scudder, M. L. *J. Am. Chem. Soc.* **1984**, *106*, 6285.
(14) Cumberland, S. L.; Hanif, K. M.; Javier, A.; Khitrov, G. A.; Strouse, G. F.; Woessner, S. M.; Yun, C. S. *Chem. Mater.* **2002**, *14*, 1576−1584.
(15) Meulenberg, R. W.; Bryan, J. D.; Strouse, G. F., unpublished results.

(e) Inductively Coupled Plasma Atomic Emission Spectroscopy. Inductively coupled plasma atomic emission spectroscopy (Thermo-Jarrell Ash IRIS) for elemental analysis was performed on the $Cd_{1-x}Co_xSe$ QD samples. Samples were dissolved in a 2% HNO_3 solution, and the Cd and Co concentrations were measured against known Cd and Co standards (High Purity Standards). The Cd emission was monitored at 214.438 and 226.502 nm, and the Co emission was monitored at 228.616, 237.862, and 238.892 nm. The reported doping percentages are averages of 3−5 runs with an error of 4−5%.

(f) Superconducting Quantum Interference Devices (SQUID). Direct current susceptibility measurements on powder QD samples were made in the 1.8−300 K region by using a superconducting quantum interference device magnetometer (Quantum Design, model 1802) at magnetic fields $H < 7$ T. Field-dependent magnetization (hysteresis loops) was performed at 2 K from −7 to 7 T.

Results and Discussion

The development of synthetic methodologies that allow production of paramagnetic ion-doped quantum dots is important for application of these materials in magnetic device technologies. Analysis of statistical doping by random displacement of core lattice points by a guest ion in these materials is a recurrent issue in DMS and in p- and n-doped materials grown by ion implantation or epitaxial methodology. Recent efforts on paramagnetic ion doping of II−VI QD materials have proven successful for Mn^{2+} and Co^{2+} doping; however, the doping levels are typically low (∼1−10%) in comparison to the levels achievable in bulk systems for transition metal ions, Mn^{2+} ($x \approx 0.8$), Fe^{2+} ($x \approx 0.2$), and Co^{2+} ($x \approx 0.4$).[3,4,8−11] Changes in the lattice, structure, magnetic, and photophysical data with increasing doping is expected in DMS materials. This suggests that correlation of the shifts in lattice parameters generated from pXRD measurements coupled to analysis of the magnetic behavior and longitudinal optical phonon modes should provide clear evidence of statistical doping in these materials, as well as provide insight into the nature of the changes in spin exchange for quantum-confined materials.

Preparation of $Cd_{1-x}Co_xSe$. To confirm that the measured Co^{2+} concentration reflects substitution of internal core Cd sites rather than surface-adsorbed Co^{2+}, the samples were repeatedly pyridine stripped. Pyridine stripping has previously been used to remove surface-bound contamination in doped QDs.[8] The doping concentrations measured by ICP-AE after pyridine stripping yield doping concentrations of $x = 0$, 0.004, 0.12, 0.17, and 0.30 mole of cobalt in $Cd_{1-x}Co_xSe$. The difference between Co concentrations in as-grown and pyridine-capped QDs are ∼10%, suggesting that surface-adsorbed Co can be removed by pyridine stripping. The mole percent of Co^{2+} can be converted to the number, n, of Co atoms per dot (∼3368 atoms/50 Å dot), predicting $n \approx 7$ for $x = 0.004$, $n \approx 202$ for $x = 0.12$, $n \approx 286$ for $x = 0.17$, and $n \approx 505$ for $x = 0.30$ Co PM spins per 50 Å CdSe QD. Using the surface-to-volume ratio for a 50 Å QD (∼20%), this predicts for the $x = 0.12$ sample, on average, that ∼40 Co ions may be isolated at the QD surface.

Our synthetic methods yield $Cd_{1-x}Co_xSe$ QDs (Figure 1) of approximately 50 Å (±2.5 Å) in diameter based on TEM analysis. Representative TEM analysis of $Cd_{1-x}Co_xSe$ nanocrystals exhibiting lattice fringes is seen in Figure 1. Based on TEM analysis, the QDs grow as spherical wurtzite crystals with an ∼5% rms size distribution. The average size and size distribution for the nanocrystals determined from the micrographs correlate with those predicted from the position and line

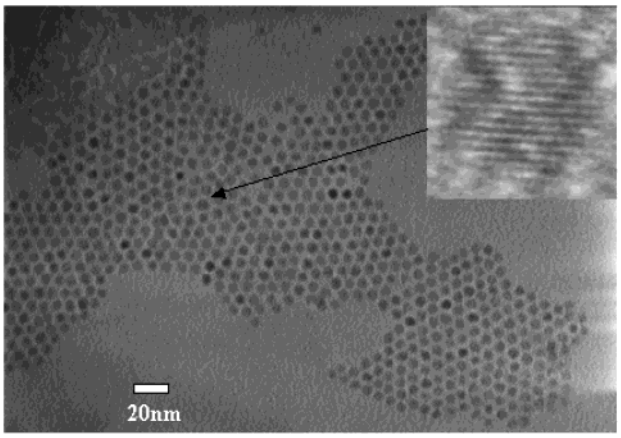

Figure 1. TEM images of hexagonally packed ∼50 Å $Cd_{0.88}Co_{0.12}Se$ QDs. Inset: Enlarged image of a single QD showing ⟨100⟩ lattice fringes. The ⟨100⟩ lattice spacing is ∼37 pm, which correlates with the ⟨100⟩ spacing observed in pXRD.

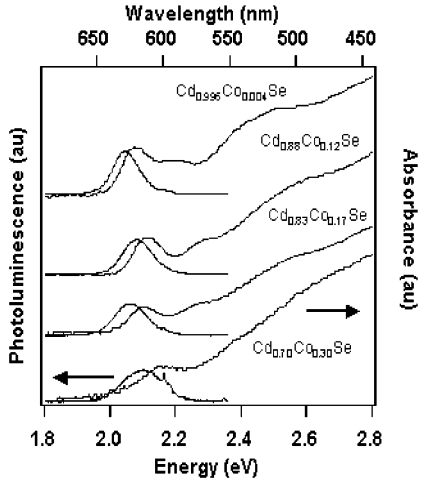

Figure 2. Absorption and photoluminescence (PL) spectra of ∼50 Å CdCoSe QDs.

width of the exciton absorption and photoluminescence (PL) band in Figure 2. The exact QD sizes are as follow: for $x = 0.004$, 5.3 Å; for $x = 0.12$, 4.9 Å; for $x = 0.17$, 5.0 Å; and for $x = 0.30$, 4.4 Å. As can be seen from this list, the dots are nearly ∼5.0 Å, with the exception of $x = 0.30$, for which the mean diameter is slightly below 5.0 Å, giving rise to the larger optical shift. The slight size changes are the cause for the observed blue shifts in the optical absorption data. These materials exhibit a small Stokes shift (30−40 meV) of the PL along with a narrow full width at half-maximum (90−100 meV). The quantum yields (QYs) for PL of these materials are 0.10, 0.19, 0.03, and 0.14 for the $x = 0.004$, 0.12, 0.17, and 0.30 doped samples, respectively. The lower QY for the $x = 0.17$ sample is surprising and may be due to dopant-induced QD stress, resulting in an increase in trap (defect) density. The photophysical behavior of these materials is currently under investigation.

Structural Analysis of $Cd_{1-x}Co_xSe$ QDs. Vegard and Schjelderup discovered in 1917 that doped single crystals do not produce a diffraction pattern with two resolved peaks, but rather a single maximum with a Bragg reflection lying between those of the components. [16] The observed Bragg reflection is

(16) Vegard, L.; Schjelderup, H. *Phys. Z.* **1917**, *18*, 93−96.

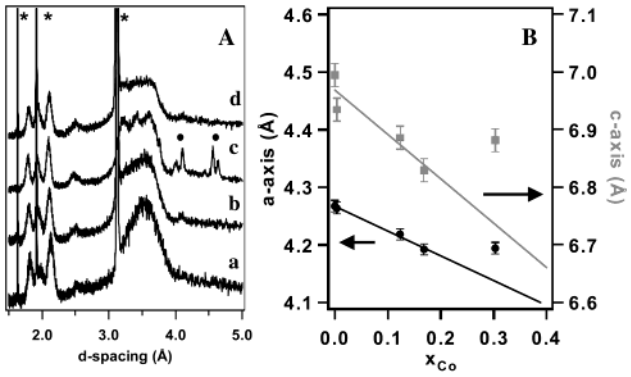

Figure 3. (A) Powder X-ray diffraction measurements for (a) $x = 0.004$, (b) $x = 0.12$, (c) $x = 0.17$, and (d) $x = 0.30$. The asterisk (∗) and circle (●) represent the Si standard and hexadecylamine diffraction peaks, respectively. (B) Shift of the a (●) and c (■) axes as a function of Co concentration. The lines are a least-squares fit to the data below $x = 0.30$.

Table 1. Cd−Se and Co−Se Bond Lengths (Å) as a Function of Concentration

x	c_{CdSe}	c_{CoSe}[a]
0	2.621	
0.004	2.608	
0.12	2.585	
0.17	2.566	
0.30	2.583	
1	2.28	2.43

[a] Reference 16.

for the average lattice parameter of the doped materials and varies linearly with dopant concentration due to the relative change in volume from the two individual components. Breaks from linearity can arise due to a structural phase transition or, in extreme cases, phase segregation, which leads to the observation of both the bulk guest and bulk host lattices in the pXRD data. Vegard's law has been applied to bulk DMS materials and recently Mn^{2+}-doped CdS QDs and shown to vary linearly for paramagnetic ion doping in a range of II−VI semiconductor systems.[17]

pXRD data are presented in Figure 3a and b for the series of doped 50 Å $Cd_{1-x}Co_xSe$ QDs. The pXRD pattern is assignable to contributions from a wurtzite lattice, without any apparent contributions from a CoSe phase. The data exhibit a linear regime for doping concentrations below $x < 0.2$ and a break from linearity at the highest doping concentration ($x = 0.30$). In the low doping regime ($x < 0.2$), a linear compression in both the a and c axes is observed, consistent with the expectations for Vegard's law behavior. The average compression of ∼11% for the calculated Cd−Cd lattice spacing (Table 1) is consistent with doping of the smaller cobalt ion (∼15% size mismatch) into a cadmium lattice point based on a simple ionic displacement model. This results in a predicted Co−Se bond distance at $x = 1$ of 2.28 Å, which is close to the observed value of 2.43 Å for the Co−Se bond distances in bulk CoSe.[18] The upper value for linear Vegard's law behavior for Co^{2+} doping of bulk CdSe is $x = 0.18$. Above $x = 0.17$, no shift in the lattice parameters for Co-doped CdSe QD samples is observed, consistent with the observation of a structural anomaly

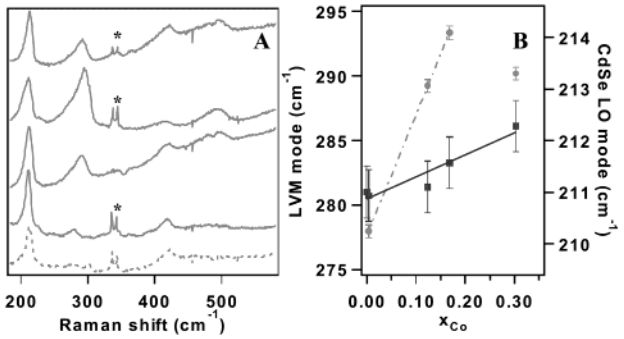

Figure 4. (A) Resonance Raman spectra for (a) $x = 0.004$, (b) $x = 0.12$, (c) $x = 0.17$, and (d) $x = 0.30$. The dashed line represents undoped CdSe QD. The asterisks (∗) represent laser plasma lines. (B) Shift of the CdSe LO mode (■) and the LVM mode (●) as a function of Co concentration. The lines are a least-squares fit to the data points.

for the CdCoSe $x = 0.30$ QD material.[19] Although this may be assignable to a ternary phase, the lack of new peaks in the pXRD makes assignment of the new phase for $x = 0.3$ difficult.

While the pXRD measures the average lattice shift for the $Cd_{1-x}Co_xSe$ samples, individual QD fringe spacing TEM analysis allows direct observation of changes in the lattice for individual QDs. Inspection of the TEM images for doped QDs indicates a surprising level of agreement between the pXRD measured lattice shifts and the changes of doping concentration in the TEM lattice fringe patterns. For $x = 0.12$, the average observed TEM lattice fringe spacing for the ⟨100⟩ plane is $d \approx$ 37 pm, which is in good agreement with the observed ⟨100⟩ spacing from pXRD analysis ($d \approx 36.5$ pm). Analysis of a large number of QDs of the TEM confirms that the pXRD values appear to reflect the total ensemble of materials.

The observed lattice changes with increasing dopant ion can also be corroborated by inspection of the shift in the longitudinal optical phonon mode (LO) for CdSe with increasing Co ion concentration. Using a simple Hooke's law analysis, systematic changes for the Brillouin zone center ($k = 0$) LO mode are expected to track the changes in the lattice arising form random displacement of Cd by Co ions. The observed mode hardening cannot be assigned to phonon confinement effects, since phonon confinement results in a relaxation of the $k = 0$ selection rule. Phonon confinement would account for the low-frequency band asymmetry but would be expected to give rise to a softening of the mode relative to the bulk (due to the low-frequency modes being removed and causing the center of mass of the phonon mode to shift red), which is opposite of the experimental observations.[20]

Coupled to the changes in the LO mode, localized vibrational modes (LVMs) may arise due to the Co substitutions in the lattice. The resonance Raman spectra, seen in Figure 4, show a hardening of the CdSe LO mode, consistent with the observed average decrease in Cd−Cd lattice spacing measured by pXRD. Coupled to the LO mode hardening, an asymmetry to lower frequency is observed in the LO mode, and two new modes, a LVM at 275 cm^{-1} and a second mode at ∼490 cm^{-1}, can be identified. For concentrations $x < 0.18$, the LVM tracks the experimental cobalt doping concentration. Above $x > 0.18$, a

(17) Jun, Y. W.; Jung, Y. Y.; Cheon, J. *J. Am. Chem. Soc.* **2002**, *124*, 615−619.
(18) Lawniczak-Jablonska, K.; Libera, J.; Iwanowski, R. J. *J. Alloys Compds.* **1999**, *286*, 89−92.
(19) Niu, C. M.; Kershaw, R.; Dwight, K.; Wold, A. *J. Solid State Chem.* **1990**, *85*, 262−269.
(20) Shiang, J. J.; Risbud, S. H.; Alivisatos, A. P. *J. Chem. Phys.* **1993**, *98*, 8432−8442.

loss of LVM intensity is coupled to a significant softening of the LVM, as predicted for a structural anomaly arising from a phase transition (as suggested in the pXRD results).

The LVM mode at 275 cm^{-1} cannot be assigned to a pure Co−Se signature based upon a modified Mazur, Montroll, and Potts (MMP) model,[21] which predicts that the frequency of a cobalt ion substituting into a cadmium lattice point will give rise to a mode at ∼198 cm^{-1}. The calculated MMP frequency may give rise to the increased asymmetry seen in the lower frequency region of the CdSe LO mode.[22] Likewise, this LVM at ∼275 cm^{-1} is not readily assignable as a LO or TO mode in the CdSe lattice, either. Although this may be assignable to a strain-induced softening of the CoSe optical phonon branch, as has been observed in $Zn_{1-x}Be_xSe$,[23] this is unlikely based upon a modified random isodisplacement model[24] for the LO mode. Using the calculated force constant for CoSe at $x = 1.0$, a strain-induced shift of the optical phonon branch would predict a shift in the frequency toward ∼215 cm^{-1} with increasing concentration, which is not experimentally observed.

A more likely explanation for the identity of this LVM mode is a mode arising from either an anharmonic lattice[25] or an electron−LO phonon coupled mode. The existence of an el−ph coupled mode has previously been identified in rare-earth-doped CdF_2,[26] with n-type doping inducing excess electrons coupled to a resultant mode softening. Furthermore, the existence of local modes arising from strong el−ph coupling in anharmonic 1-D MX crystals has also been observed.[27] The possibility of the LVM at ∼275 cm^{-1} arising from enhanced el−ph coupling in $Cd_{1-x}Co_xSe$ may be due to enhanced anharmonic effects in doped systems. The introduction of a Co^{2+} ion into a Cd^{2+} ion lattice point should induce p-type doping, with excess holes in the valence band of the QD which would lead to the observation of an el−LO phonon coupled mode arising in the vibrational spectrum.

The mode at ∼490 cm^{-1} may arise from a combination band based upon the mode frequencies of the CdSe LO mode (∼210 cm^{-1}) and the LVM mode (∼275 cm^{-1}). As the LO mode has A_1 symmetry and LVM typically has A_1 symmetry, the two modes can combine to give a new mode at $\nu_{comb} = \nu_{LO} + \nu_{LVM} \approx 485$ cm^{-1}. We note, however, that this indicates the term LVM may not be rigorously correct for the 275 cm^{-1} mode in this situation, due to the existence of the combination mode, which would suggest that a significant degree of coupling must occur in the lattice to produce the combination mode.

Electron−Phonon Coupling in $Cd_{1-x}Co_xSe$. The possibility for strong coupling arising from changes in the el−ph interactions in doped materials can be analyzed by inspection of the overtone modes in the Raman data in Figure 4. Analysis of the LO phonon and phonon replicas provides an indirect measurement of the magnitude of the el−ph coupling in $Cd_{1-x}Co_xSe$ by calculation of the Huang−Rhys parameter, *S*, a measure of the distortion between the ground- and excited-state manifold. Assuming that the intensities of the given transition can be used in place of the transition probabilities, *S* can be directly calculated from the vibrational data. [20] *S* is given by

$$\frac{P_{a\rightarrow b_i}}{P_{ab}} = \frac{S^i e^{-S}}{i!} \tag{1}$$

where $P_{a\rightarrow b_i}/P_{ab}$ is the relative transition probability for the *i*th phonon replica. [28] The intensity of the Raman experiment is given by[2929]

$$I_{a\rightarrow b} = c(\nu_o \pm \nu_{ab})^4 \sum_{\rho\sigma} |(P_{\rho\sigma})_{ab}|^2 \tag{2}$$

which is directly proportional to the transition probability P_{ab}. Assuming that $I \propto P$ (i.e., low-power condition), the calculation of *S* will be given by $I_{LO}/I_{2LO} = 2/S$.[25] The values of S_n (n = CdSe LO or LVM mode) as a function of concentration are shown in Table 2. Interestingly, all the calculated values of S_{LO} are above the value of 2.36 for undoped 50 Å CdSe, which is consistent with increased el−ph interactions in the QD.[30] For $x = 0.004$, the value of S_{LO} increases by a factor of 2 relative to that of undoped CdSe but then decreases by a factor of nearly 1.7 at $x = 0.30$. The observed decrease in S_{LO} is correlated with a decrease in S_{LVM}, where S_{LVM} is a calculation for the LVM mode at 275 cm^{-1}. Between $x = 0.004$ and $x = 0.30$, the value of S_{LVM} decreases by nearly a factor of 2.5. The decrease in the value of *S* suggests that el−ph coupling is decreased with increasing cobalt concentration, possibly due to the onset of a ternary lattice for the higher doped samples, as suggested in the anomaly in the pXRD results. While these results do not clearly identify the nature of the defect mode, they suggest that changes in the el−ph coupling are consistent with the appearance of an LVM. Similar LVMs have been observed in 3d transition metal ions doped into zinc blende and wurtzite II−VI materials.[31]

Table 2. Calculated Huang−Rhys Constants from Raman Spectra

x	S_{CdSe}	S_{LVM}
0	2.36	
0.004	4.72	3.06
0.12	4.67	1.76
0.17	3.33	1.27
0.30	2.73	1.25

Magnetic Properties in $Cd_{1-x}Co_xSe$ QDs. In II−VI materials, the nature of the magnetic properties depends on the magnitude of the transition metal ion-exchange coupling with the QD electronic levels. The magnitude of mixing is dependent on the d-orbital mixing with the s and p electrons in the valence band (VB) and conduction band (CB) of the II−VI QD host. The values for the el−ph coupling constants, which can modulate the sp−d mixing in II−VI materials, suggest that significant perturbation of the QD properties may lead to unique magnetic effects. Classical behavior for DMS based on bulk Co:CdSe shows evidence for two magnetic regimes: a high-

(21) Lucovsky, G.; Brodsky, M. H.; Burstein, E. *Phys. Rev. B* **1970**, *2*, 3295−3302.
(22) Mak, C. J.; Bak, J.; Sooryakumar, R.; Steiner, M. M.; Jonker, B. T. *J. Appl. Phys.* **1994**, *75*, 5719−5724.
(23) Pages, O.; Ajjoun, M.; Laurenti, J. P.; Bormann, D.; Chauvet, C.; Tournie, E.; Faurie, J. P. *Appl. Phys. Lett.* **2000**, *77*, 519−521.
(24) Chang, I. F.; Mitra, S. S. *Phys. Rev.* **1968**, *172*, 924−933.
(25) Sievers, A. J.; Takeno, S. *Phys. Rev. Lett.* **1998**, *61*, 970−973.
(26) Eisenberger, P.; Adlerstein, M. G. *Phys. Rev. B* **1970**, *1*, 1787−1804.
(27) Swanson, B. I.; Brozik, J. A.; Love, S. P.; Strouse, G. F.; Shreve, A. P.; Bishop, A. R.; Wang, W. Z.; Salkola, M. I. *Phys. Rev. Lett.* **1999**, *82*, 3288−3291.
(28) Hehlen, M. P.; Kuditcher, A.; Rand, S. C.; Tischler, M. A. *J. Chem. Phys.* **1997**, *107*, 4886−4892.
(29) Nakamoto, K. *Infrared and Raman spectra of inorganic and coordination compounds*, 5th ed.; Wiley: New York, 1997.
(30) Meulenberg, R. W.; Strouse, G. F. *Phys. Rev. B* **2002**, *66*, 035317.
(31) Mayur, A. J.; Sciacca, M. D.; Kim, H. J.; Miotkowski, I.; Ramdas, A. K.; Rodriguez, S. *Phys. Rev. B−Condensed Matter* **1996**, *53*, 12884−12888.

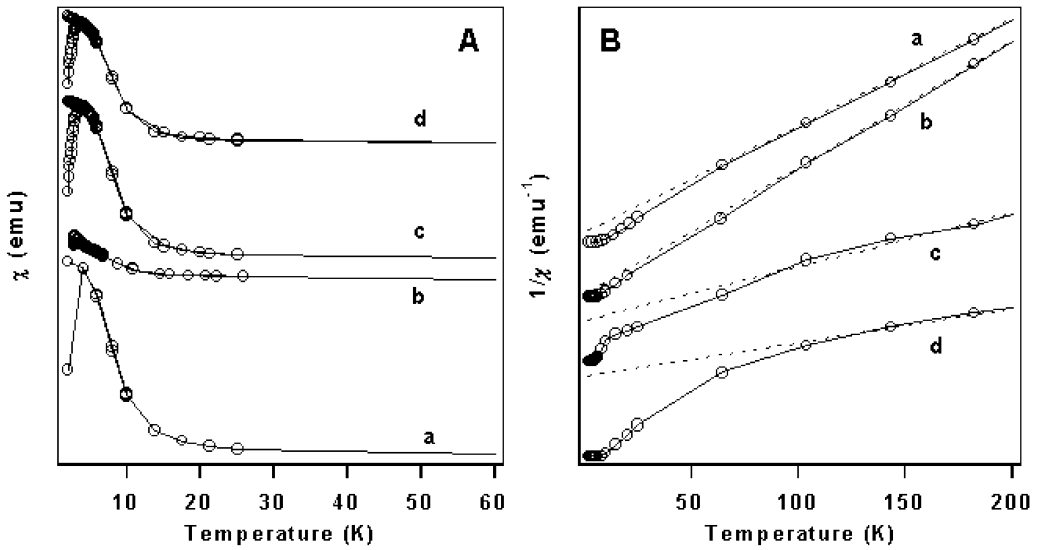

Figure 5. (A) Magnetic susceptibility (ZFC and FC; $B = 500$ Oe) versus temperature and (B) inverse magnetic susceptibility versus temperature for (a) $x = 0.004$, (b) $x = 0.12$, (c) $x = 0.16$, and (d) $x = 0.30$. The lines are a least-squares fit to the high-temperature part of the trace and are consistent with Curie−Weiss behavior.

temperature PM regime and a low-temperature SG-AFM regime.[1] Traditionally, magnetic studies on bulk Co−DMS systems show very low spin-glass temperatures ($T_g < 1$ K) and no deviations in specific heat measurements. Curie−Weiss behavior in the high-temperature regime of these systems followed by a transition to AFM coupling of the cobalt ions has been observed. To explain the onset of AFM coupling, a superexchange (SE) mechanism between nearest-neighbor (J_{NN}) Co pairs has been suggested due to a strong radial exchange interaction ($J(R)$) of the spin $S = {}^3/_2$ system.[3]

In Figure 5a, a plot of $\chi(T)$ versus temperature is shown for $Cd_{1-x}Co_xSe$ ($x = 0.004-0.30$). Analysis of the magnetic data in Figure 5a and b indicates that, in our DMQD systems, the high-temperature phase is paramagnetic and undergoes a low-temperature magnetic phase transition, as evident in the cusp (between 2 and 4 K) seen in the direct current susceptibility data. A plot of $1/\chi(T)$ (Figure 5b) indicates classical Curie−Weiss behavior at high temperature, consistent with uncoupled PM behavior in the lattice. With increasing Co concentration, an anomaly at low temperature is observed in the $\chi(T)$ data, which can be attributed to a transition to SG behavior. This is confirmed by comparison of the zero-field-cooled (ZFC) and field-cooled (FC) data in Figure 5a. Interestingly, the "cusp" temperature, more commonly called the glass temperature (T_g), is an order of magnitude higher than values observed in bulk Co−DMS systems ($T_g \approx 100-900$ mK) of equivalent doping concentrations.[5,32] The observed increase in T_g for the Co-doped CdSe QDs potentially arises from enhanced long-range order of the cobalt ions in these systems.

The magnetic susceptibility, $\chi(T)$, at the high-temperature limit can be represented by the Curie−Weiss law, $\chi(T) = C/(T - \Theta)$, where C is the Curie constant, T is the temperature in Kelvin, and Θ is the Curie temperature. Fitting the high-temperature limit $1/\chi$(T) values to Curie−Weiss behavior, both the $x = 0.004$ and 0.12 doped samples show a positive Curie temperature (Θ), while the $x = 0.17$ and 0.30 samples show a negative Curie temperature, implying AFM interactions in the heavily doped samples (Table 3). The positive Curie temperatures suggest FM or canted AFM interactions in these materials. The observation of an AFM-SG phase suggests that the Co ions are strongly interacting in the lattice. This is analogous to the observation of strong superexchange in Co-doped bulk CdSe, arising primarily from nearest-neighbor (J_{NN}) interactions between the Co ions. Support for an AFM-SG phase in the highly doped samples is witnessed in the magnetization data, $M(H)$, where no evidence for hysteresis is seen (Figure 6). The AFM interactions can arise between Co spins in an isolated particle (intraparticle) or AFM interactions between spins in neighboring particles (interparticle). However, the organic passivating layer on the QD results in a large particle−particle spacing, resulting in a minimal contribution from interparticle coupling, and is unlikely to be the dominant contribution to the observed AFM signal.

Table 3. Nearest-Neighbor $Co^{2+}-Co^{2+}$ Curie Temperatures (Θ) and Exchange Integrals (J_{NN}) for $Cd_{1-x}Co_xSe$ QDs

x	Θ (K)	J_{NN} (K)
0.004	3	0.1
0.12	6	0.2
0.17	−168	−5.6
0.30	−3660	−122

The magnetization of the $x = 0.12$ sample in the inset of Figure 6 shows evidence of high field saturation, which can be described by a Langevin function,

$$\frac{M}{M_s} = \coth\left(a\frac{H}{T}\right) - \frac{T}{aH} \qquad (3)$$

where M/M_s is the relative magnetization and $a = \mu/k$. Equation 3 is obtained from the classical limit ($J = \infty$) of the Brillouin function,

$$\frac{M}{M_s} = \frac{2J+1}{2J}\coth\left(\frac{2J+1}{2J}a\frac{H}{T}\right) - \frac{1}{2J}\coth\left(\frac{a}{2J}\frac{H}{T}\right) \qquad (4)$$

where J is the total angular momentum. An effective Bohr

(32) Shand, P. M.; Lewicki, A.; Miotkowski, I.; Crooker, B. C.; Furdyna, J. K. *Phys. Rev. B−Condensed Matter* **1991**, *44*, 6152−6157.

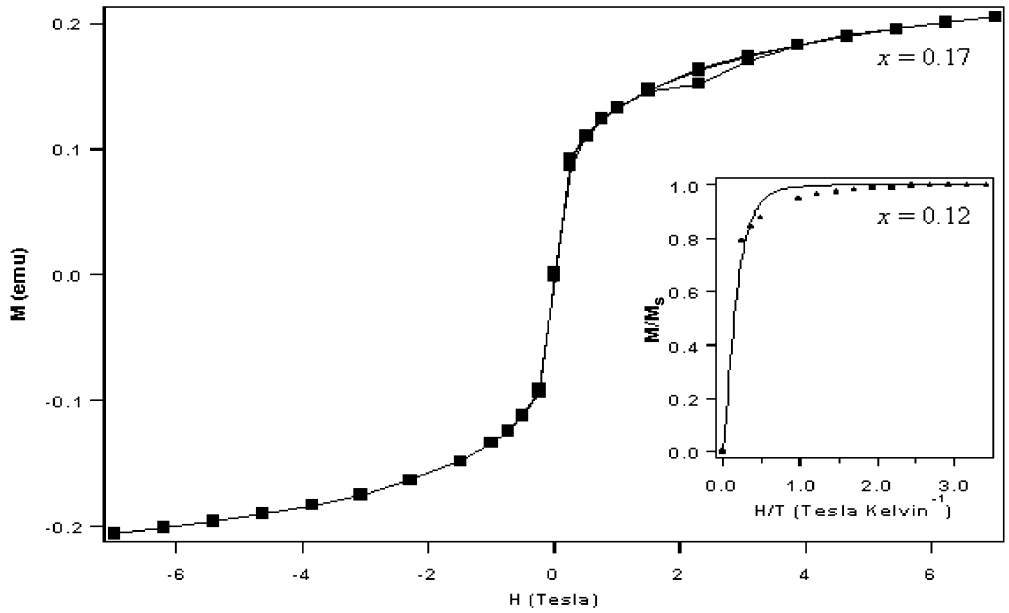

Figure 6. Field-dependent magnetization, $M(H)$, for $x = 0.17$ Co:CdSe. Inset: $M(H)$ for $x = 0.12$ Co:CdSe. The $x = 0.12$ case shows high field saturation, as expected for a paramagnet, and can be described by a Langevin function (see text).

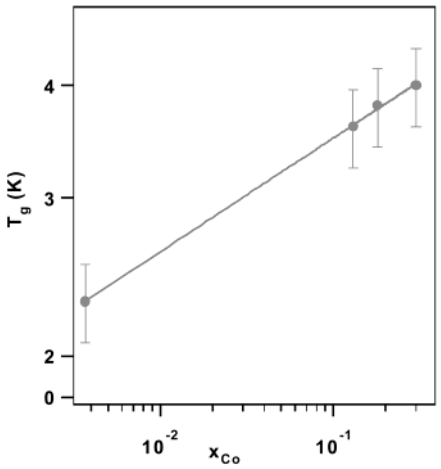

Figure 7. Plot of the glass temperature, T_g, versus Co concentration on a log−log scale. The line is fit to the power law, $T_g \sim Bx^{n/3}$, where n is the radial extent of the superexchange interaction.

magneton, μ_{eff}, of 3.52 μ_B can be obtained from the data, very close to the spin-only value of 3.87 μ_B, indicative of paramagnetic spin domains in the low-doped samples. This supports the susceptibility measurements that suggest that the low-doped samples exhibit high-temperature paramagnetic behavior with weak ferromagnetic interactions at low temperature.

The observed values for Θ as a function of the concentration of the Co ion can be assumed to represent the overall exchange integral for the Co−Co coupling and can be used as an estimate for the SE interaction strength in these materials. The magnitude of the SE interaction for DMQD systems can be obtained by fitting the concentration dependence of T_g.[3] As de Jonge and co-workers have observed, DMS systems typically follow a power law behavior governed by $T_g \sim Bx^{n/3}$, where B is a constant and n represents the radial dependence of the SE interaction (Figure 7). For the Co:CdSe QD systems, fitting T_g to a SE model yields $n = 0.38$, which is an order of magnitude smaller than the values observed in bulk Co−DMS systems. The decrease in n by an order of magnitude is surprising when

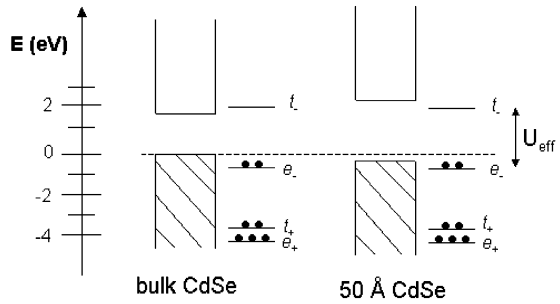

Figure 8. Schematic illustration of the Co^{2+} energy levels in (a) bulk CdSe and (b) a 50 Å CdSe QD.

compared to bulk values that typically range from 6.3 in bulk Co−DMS to 6.8 for bulk Mn-DMS, or 12 for bulk Fe−DMS.[3] If we assume that the coupling is dominated by NN interactions, the smaller value can be understood by expressing the radial dependence of the exchange interaction, n, in terms of $J_1 \sim J_{NN}R^{-n}$. For small values of n, this implies an increased long-range coupling of the spins in the system. The concentration-dependent nearest-neighbor exchange constants, J_{NN}/k, can then be calculated from the equation $J_{NN}/k = 3\Theta/2ZS(S + 1)$, where S is the spin and Z is the number of nearest neighbors.[1] Values of J_{NN}/k are calculated for the values of x and listed in Table 3.

The values of J_{NN} correlate with the doping concentration, which suggests that an enhanced SE interaction with increasing Co^{2+} concentration is observed in these QD materials. This is similar to what has been seen of Mn-doped CdS nanoparticles.[6] This suggests that the increases in J_{NN} may arise from stronger hybridization of the d-orbitals of the Co^{2+} with the CdSe QD valence band in comparison to bulk CdSe.[3] As illustrated in Figure 8, in the bulk CdSe lattice, the occupied e_+ and t_+ orbitals lie ~4 eV below the valence band while the occupied e_- orbital lies ~800 meV below the valence band. However, as the particle size become smaller, the VB and CB shift according to the following scaling laws: $E_{VB} \sim r^{-1.24}$ and $E_{CB} \sim r^{-1.37}$.[33]

(33) Williamson, A. J.; Zunger, A. *Phys. Rev. B* **2000**, *61*, 1978−1991.

Therefore, a 50 Å particle exhibits a VB shift of ~190 meV with a shift of ~210 meV of the CB. This shift of 191 meV increases the orbital overlap integral between the Co^{2+} d-orbitals and the CdSe VB and may explain the observed increase in the experimental J_{NN} exchange integral for the Co-doped CdSe QDs.

The contribution of Co d-orbital hybridization with the valence band of the host material can be calculated for a 50 Å $Cd_{1-x}Co_xSe$ QD using

$$N_o\beta_{hyb} = 32V_{pd}^2\left(\frac{U_{eff}}{(e_- + U_{eff} - E_{VB})(E_{VB} - e_-)}\right) \quad (5)$$

where V_{pd} is the hybridization parameter (~1 eV), e_- are the occupied Co^{2+} levels, E_{VB} is the valence band energy, and U_{eff} is defined as the energy difference between the occupied (e_-) and unoccupied (t_-) Co orbitals. For bulk CdSe, assuming $E_{VB} = 0$ eV, $e_- \approx 0.8$ eV, and $U_{eff} \approx 2.8$ eV, the estimated value for $N_o\beta_{hyb} \approx -31.1$ eV.[34] For a 50 Å CdSe QD, assuming the size-dependent shift in the VB energy is $E_{VB}(QD) \approx [E_{VB}(bulk) - 0.19$ eV], the $N_o\beta_{hyb}(QD)$ can be estimated for a 50 Å $Cd_{1-x}Co_xSe$ QD to be ~ −43.1 eV. The change in the overlap of the d-orbitals and the CdSe VB is ~30% greater at particle sizes of ~50 Å when compared to bulk CdSe, which can account for the observed increase in the NN exchange interaction.

An alternative possibility for enhanced magnetic coupling in QDs is the potential for longer-range contributions arising from J_{NNN} and J_{NNNN} interactions. Figure 9 shows the long-range dependence of J_1 for bulk Co:CdSe and the estimated values for a 50 Å Co:CdSe QD. The line in Figure 9 is the empirical fit to the SE model, while the J_{NNN} and J_{NNNN} values were calculated assuming that the long-range exchange interactions in the QD occur at the same $Co^{2+}-Co^{2+}$ distances (R) as seen in the bulk. As the model shows, the expected values for J_{NNN} and J_{NNNN} are an order of magnitude higher than what is witnessed in the bulk DMS system. The enhancement of J_{NNN} and J_{NNNN} is intriguing and may arise from changes in el−ph coupling with increasing dopant concentration, which may cause an increase in T_g consistent with recent calculations.[35] This could result in spin domains forming in the QD lattice, which would influence coupling. In addition, the large values of Θ imply that a simple least-squares application of the Curie−Weiss law to the high-temperature susceptibility may not be adequate in describing the interactions in these materials. [36] This has been observed in materials that exhibit longer-range magnetic coupling from NNN and NNNN interactions.[37]

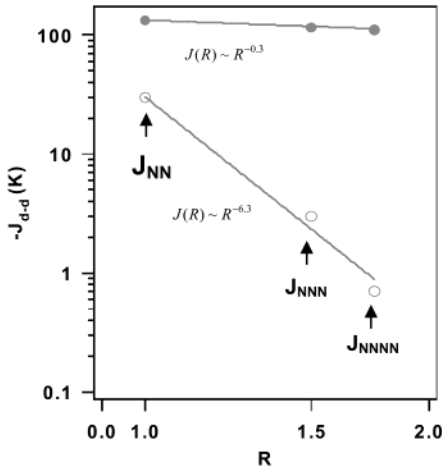

Figure 9. Radial extent of the exchange interaction, *J(R)*, versus the dopant−dopant distance in the crystal. The lower trace is for bulk Co:CdSe from ref 3, and the upper trace is for the $Cd_{0.70}Co_{0.30}Se$ QD samples. Note that the smaller value of *n* in the QD samples implies a much longer superexchange interaction.

Conclusions

Random ion displacement of core Cd^{2+} sites by Co^{2+} ions in CdSe QDs can be achieved. pXRD data coupled to Raman spectroscopy confirm a linear lattice compression with increasing Co concentration in accord with Vegard's law. The observed hardening of the LO phonon mode and an appearance of a local vibrational mode at 275 cm^{-1} suggest that changes in the el−ph coupling may arise in these materials with increasing Co^{2+} concentration. Coupled to changes in the el−ph interaction, an enhancement of longer-range superexchange interactions arises. Surprisingly, the values for J_{NN} are increased by an order of magnitude in the QD when compared to those in the bulk, which may result from an increase in Co d-orbital overlap with the CdSe valence band minimum. Further studies into the magnetics and dynamics of these diluted magnetic quantum dots are underway.

Acknowledgment. This work was supported by a NSF-CAREER Award (DMR-9875940). We acknowledge Dr. Henrik Birkedal and Dr. J. Daniel Bryan for corroborating our pXRD results by Reitveld refinement analysis of the data set.

JA0262840

(34) The difference between our calculated coupling term (−31.1 eV) and the experimental coupling term (−1.87 eV) may occur from the use of $E_v = 0$, from V_{pd} changing with dopant ion, or from U_{eff} not reflecting the true values of the dopant ions in the nanocrystal. Although the calculated values may not be rigorously correct, the observed trends from the calculations, however, are important.

(35) Li, M. Z.; Zou, L. J.; Zheng, Q. Q. *J. Appl. Phys.* **1998**, *83*, 6596−6598.

(36) Srdanov, V. I.; Stucky, G. D.; Lippmaa, E.; Engelhardt, G. *Phys. Rev. Lett.* **1998**, *80*, 2449−2452.

(37) Rushbrooke, G. S.; Baker, G. A.; Wood, P. J. In *Heisenberg model*; Domb, C., Green, M. S., Eds.; Academic: London, 1974; Vol. 3, pp 245−356.